A&A 394, 603–615 (2002)
DOI: 10.1051/0004-6361:20021154

Astronomy & Astrophysics

Identification of non-radial pulsation modes in the close-binary β Cephei star ν Centauri*

C. Schrijvers[1,2] and J. H. Telting[3]

[1] Astronomical Institute Anton Pannekoek, University of Amsterdam, and Center for High Energy Astrophysics, Kruislaan 403, 1098 SJ Amsterdam, The Netherlands
[2] Space Department, TNO TPD, Stieltjesweg 1, 2600 AD Delft, The Netherlands
e-mail: schrijvers@tpd.tno.nl
[3] Nordic Optical Telescope, 38700 Santa Cruz de La Palma, Spain
e-mail: jht@not.iac.es

Received 2 April 2001 / Accepted 7 August 2002

Abstract. We present time series of high-resolution spectra of the β Cephei star ν Cen, showing multi-periodic variations in the Si III λ 4552 and λ 4567 line profiles. After correction for the binary motion, we analyse the time series of spectra by Fourier transforms for each position in the line profile. For selected frequencies we perform a direct fit of multiple sinusoids. Four frequencies are needed to describe the pattern of moving bumps in the line profiles. We present the distributions of variational amplitude and phase across the line profile and use these diagnostics to show that most of the variability can be explained by multiple non-radial pulsations. From the phase distributions across the line profiles we derive estimates for the degree ℓ of the individual pulsation modes in ν Cen. We find ℓ values ranging from 6 to 10. We find no trace of a previously reported low-degree $\ell \lesssim 2$ pulsation with a period of 0.17 day. We briefly discuss these observations, and those of the other close-binary β Cephei stars α Vir and ψ^2 Ori, in terms of tidal effects on pulsation-mode stability.

Key words. line: profiles – stars: early-type, oscillations, rotation – stars: variables: β Cephei stars – stars: individual: ν Cen

1. Introduction

The number of β Cephei stars which are found to vary multi-periodically is rapidly increasing. In many cases the variability found in these stars is succesfully explained by models of stellar oscillations. The presence of multiple non-radial pulsation modes, which penetrate the stars interior, offers the means to test and improve theories of stellar structure and evolution. The β Cephei stars are therefore excellent candidates for asteroseismological applications.

In this paper we present a time series of high-resolution spectra of ν Cen (HD120307, $m_V = 3.41$, B2IV). ν Cen is a single-line spectroscopic binary (Palmer 1906). Orbital elements were first determined by Wilson (1914) who obtained a circular orbit with $P = 2.62516$ day. Double emission surrounding the absorption core of Hα was found by Hendry & Bahng (1981), which means that ν Cen may be classified as a Be star. It is probable that the emission is not an intrinsic property of the star but the result of binary interaction (Cuypers et al. 1989).

The β Cephei character of the primary of ν Cen was discovered by Rajamohan (1977) and later confirmed by Kubiak & Seggwiss (1982), Ashoka et al. (1985) and Ashoka & Padmini (1992). In the O–C variations of their measured radial velocities around the orbital solution they detected β Cephei-type variation with a pulsation period of $P \sim 0.17$ day. Ashoka & Padmini showed that in 1985, 1987 and 1988 a pulsation with this period gave rise to a radial velocity amplitude of about 10 km s^{-1}, and that this mode can be traced back in earlier data sets, such as that of Kubiak & Seggwiss, albeit with a lower amplitude. Ashoka & Padmini argued that the difference in amplitude is not likely to be due to beating of two modes with similar frequencies, as their data taken at the 3 different epochs shows consistent velocity amplitude: the difference is probably due to the use of different observing instrumentation and different absorption lines, some of which might be affected by emission. Small-amplitude light variations, with period 0.17 day, were found in two nights of data presented by Kubiak & Seggwiss (1982): $\Delta u = 8$ mmag, but the other Strömgren bands showed no systematic changes. Cuypers et al. (1989) found no photometric variations with amplitudes exceeding 2 mmag in Strömgren b at frequencies other than the orbital frequency. Note that the Cuypers et al. data were taken very close in time to the 1987 and 1988 spectroscopic data of Ashoka & Padmini (1992). These amplitudes of light and

Send offprint requests to: J. Telting, e-mail: jht@not.iac.es
* Based on data taken at ESO La Silla.

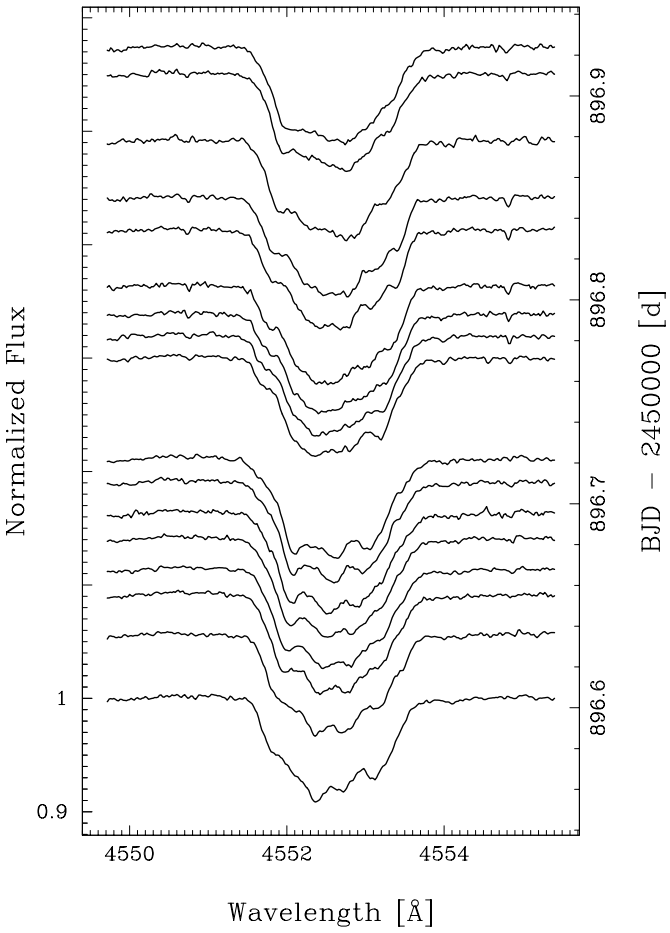

Fig. 1. One night of data of the λ4552 line profile. Spectra are offset according to acquisition time. The line profiles are corrected for orbital velocity shifts. The moving bumps visible in the first half of this night seem to disappear gradually. At the second half of the night the number of moving bumps and their amplitude have decreased. Such behavior can be explained by multiple non-radial pulsation modes: modes with similar ℓ values cooperate in the beginning of the night, while at the end of the night the modes cancel reveiling or mimicing a mode with much lower ℓ value.

radial velocity variations hint to a non-radial pulsation mode of low degree, $\ell = 1$ or $\ell = 2$.

Waelkens & Rufener (1983) suggested that tidal interactions have a damping effect on β Cephei type pulsations, which would explain the then observed lower limit of the orbital periods of the binary β Cephei stars (they considered α Vir the β Cephei star with the shortest known orbital period, P = 4.02 day). In an attempt to find β Cephei type variability in stars with orbital periods shorter than that of α Vir, they photometrically observed 16 short-period binaries that are inside or close to the β Cephei star instability strip, but found no new pulsating cases for $P < 4$ day. The present work on ν Cen shows, as well as the above described investigations, that β Cephei stars with shorter orbital periods *do* exist. Another such case was presented by Telting et al. (2001) for the star ψ^2 Ori, which has an orbital period $P = 2.53$ day: its primary shows, like in ν Cen and α Vir, a clear moving-bump pattern in its absorption lines. To the best of our knowledge, the two binary systems ψ^2 Ori and ν Cen present the β Cephei stars with the shortest orbital periods presently known.

Brown & Verschueren (1997) have determined a projected rotational velocity $V_e \sin i$ of 65 ± 6 km s^{-1} using an artificially broadened sharp-lined template spectrum matching the measured FWHM of weak metal lines. De Geus et al. (1989) have analysed Walraven photometry of the members of the Sco-Cen OB 2 association, and for ν Cen they derived $\log T_{\rm eff}$ = 4.35, $\log g$ = 4.02, and $\log L/L_\odot$ = 3.7. These values place ν Cen inside the domain of the Hertzsprung-Russell diagram where β Cephei stars are predicted to be unstable against non-radial pulsations (Dziembowski & Pamyatnykh 1993). Fundamental stellar parameters were also derived by Remie & Lamers (1982), who combined various observational data with model atmosphere and stellar evolution codes; they found $R/R_\odot$ = 6.7, $M/M_\odot$ = 13, d = 190 pc, $\log T_{\rm eff}$ = 4.352, $\log g$ = 3.90 and $\log L/L_\odot$ = 4.02. De Zeeuw et al. (1999) used the Hipparcos parallax, 6.9 ± 0.8 mas, and proper motion to identify ν Cen with 99% probability as a member of the Upper Centaurus Lupus association, which has a mean distance of 140±2 parsec.

In this paper we show that the primary in ν Cen exhibits multi-periodic variations of the Si III λ4552 Å and λ4567 Å line profiles. We show features moving from blue to red across the line profiles on time scales of several hours, that are typical for non-radial pulsations. To the best of our knowledge this is the first time that high-resolution spectroscopic time series of line profiles of ν Cen have been presented in the literature. We also show that in our data, taken in 1998, we find no trace of the low-degree pulsation mode (period 0.17 day) that was apparent in datasets taken throughout a major part of the 20th century.

In Sect. 2 we describe the acquisition and reduction of the data. We measure the equivalent width and radial velocity variations in Sects. 3 and 4; from the latter we determine the orbital parameters. In Sect. 5 we discuss the line-profile variations. In Sect. 6 we apply three different methods to analyse the intensity variations at each position in the line profile: Fourier analysis, multiple-sinusoid fit and single-sinusoid fits. With these three techniques we create diagnostic diagrams that allow to estimate the ℓ value of the responsible non-radial pulsation modes in Sect. 7. In Sect. 8 we discuss the implications and restrictions posed by the explanation of non-radial pulsations as the main cause for the line-profile variability in ν Cen. In Sect. 9 we discuss these new observations of ν Cen regarding possible tidal effects. We formulate conclusions in Sect. 10.

2. Observations and reduction

In March 1998 we obtained 93 high-resolution spectra (R = 65 000) of ν Cen at the ESO La Silla observatory with the CAT telescope and the CES spectrograph. The spectral range, projected by the long camera on about 2600 useful columns of CCD #38, covers the Si III triplet λ4552, 4567, 4574 Å. The total time span of the acquired time series is 9.26 day. Exposure times were typically 12 min and were kept shorter than 20 min, resulting in S/N ratios of the reduced spectra typically between 600 and 1200.

The spectra were reduced using standard packages in IRAF. Wavelength calibration was done with ThAr calibration

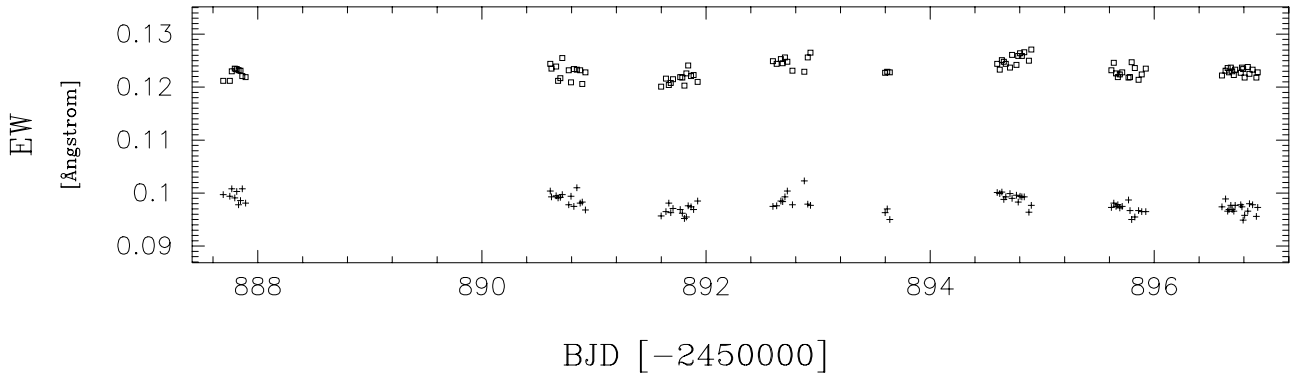

Fig. 2. Variation of the equivalent width of the λ 4552 (open squares) and the λ 4567 line profile (plus symbols).

spectra. We used the CCD overscan region to determine the bias level. CCD pixel-to-pixel variations were removed by flat fielding with dome flats; dome flats also provided a first rough correction for the continuum shape which is heavily affected by vignetting of the light beam. Bad columns were removed by linear interpolation of pixel intensities in adjacent columns. One-dimensional spectra were extracted after subtracting a global fit to background and scattered light. All spectra were shifted to, and acquisition times were transformed to the barycentric frame. We normalized the spectra by fitting a cubic spline with typically 10–15 segments to the regions in between the obvious absorption lines in the extracted spectra. For our analysis we used only the λ 4552 and λ 4567 lines, since these two lines of the triplet have the highest quality in our data.

3. Analysis of the equivalent width

We calculated the equivalent width (EW) for the λ 4552 and λ 4567 lines in the way described in Schrijvers et al. (1997, hereafter referred to as S97). The integration domains were chosen separately for each observing night, based on where the average line profile for that night reaches the continuum. The measured EW values are shown in Fig. 2.

The fact that both lines are of the same triplet means that if the measured EW variations were real, i.e. not caused by noise and/or errors from the reduction process, the variations in both lines should be correlated. However, the EW measured from the λ 4552 and λ 4567 lines show small variations that seem unrelated. We suspect that the EW variability is mainly caused by errors in the normalization of the spectra. A small part of the variability is possibly linked to orbital phase (see Sect. 5.1).

4. Radial velocity variations

4.1. The orbit

We calculated the radial (centroid) velocity of the line profiles as described in S97, for the rest wavelengths 4552.6 Å and 4567.8 Å. The orbit of ν Cen around its close companion is clearly visible in the radial velocity curve in Fig. 3. We computed the single-line binary orbit solution by means of the Sterne (1941) method which uses a perturbation of a circular orbit solution to fit the orbital elements. The orbit is known to be circular with a period $P = 2.625$ day (Wilson 1914), with a radial velocity semi-amplitude $K = 20.6\,\mathrm{km\,s^{-1}}$ (Lucy & Sweeney 1971). While keeping this orbital period fixed in our fit we obtained a semi-amplitude $K = 22.4 \pm 0.4\,\mathrm{km\,s^{-1}}$ for the λ 4552 line and $K = 22.2 \pm 0.4\,\mathrm{km\,s^{-1}}$ for the λ 4567 line. A fit with the period as free parameter gives identical results for both lines, $P = 2.622 \pm 0.018$ day, with the same semi-amplitude K as before. All fits for both spectral lines are consistent with a circular orbit. Given the low eccentricity we also fitted a single sinusoid to the radial velocity data.

We tried all three fits (period fixed, free, and sinusoid) to correct for the orbital Doppler shifts but found no differences in the results of our analysis of the pulsation modes. For this paper we adopted the solution from the $P = 2.622$ fit, leading to the epoch of maximum radial velocity $T_0 = 2450894.32 \pm 0.01$ day. The residual radial velocities after correcting for the orbit are displayed in the top panel of Fig. 3.

In the rest of this paper we will use the orbit-corrected spectra to analyse the intrinsic variability of the primary star in ν Cen. The line profiles show a behavior that is typical for a star exhibiting multiple non-radial pulsation modes: a complex pattern of bumps that move from the blue to the red side across the line profiles, on time scales of several hours. One night of line profiles is shown in Fig. 1. In some nights the variations seem to have disappeared while in other nights we find variations that are much larger than in this example.

4.2. A low-degree mode has damped out?

Rajamohan (1977) found β Cephei-type variation in his radial velocity O–C diagrams. He detected a period of $P \sim 0.17$ day, which was confirmed by Kubiak & Seggwiss (1982), Ashoka et al. (1985) and Ashoka & Padmini (1992).

Our radial velocity measurements are not consistent with this period: we checked if our O–C variations (top panel of Fig. 3) show variations with a similar period, but we could not confirm a period of $P \sim 0.17$ day from our data. Actually, the region in frequency space around $P \sim 0.17$ (frequency $5.9\,\mathrm{d^{-1}}$) shows hardly any variability. Note that the peak-to-peak changes in our O–C residuals are less than $4\,\mathrm{km\,s^{-1}}$, which is comparable to the projected slit width on the CCD, whereas Ashoka & Padmini clearly showed that in 1985, 1987 and 1988 the pulsation with $P \sim 0.17$ day gives rise to a

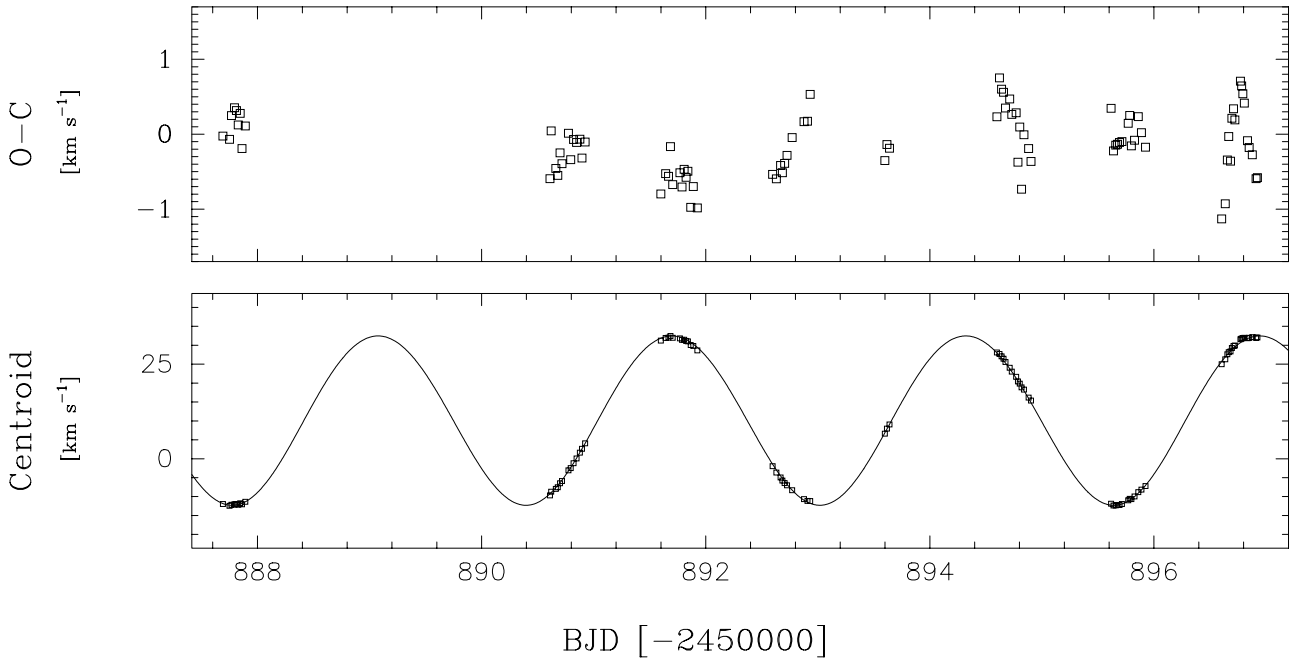

Fig. 3. Bottom: Radial velocity variations for λ 4552. **Top:** O–C diagram for λ 4552: the residual radial velocities after removal of the binary-orbit solution.

radial velocity amplitude of about 10 km s^{-1} (20 km s^{-1} peak-to-peak).

An explanation for this discrepancy could be that the data presented in the above 4 publications consisted of only a few tens of spectra, taken over several years. The spectroscopic observations typically lasted for less than 1.5 cycle per observing run, as is the case for the evidence for photometric periodicity. The radial velocities were computed from the central part of the line profiles, a method which can give rise to overestimated values of the radial velocity changes in case of pulsating stars (see e.g. De Cat et al. 2000). Furthermore, the previously observed period $P \sim 0.17$ day lies in between two of the likely candidate periods we find in our data set (see Sect. 5): given the temporal sampling of the previous low-resolution spectra, the previously determined period might have been confused by alternating dominant appearences of variations at these newly found frequencies.

Nevertheless, combining the previous low-resolution spectroscopic data sets Ashoka & Padmini (1992) convincingly showed that the $P \sim 0.17$ day mode is present in all the data they looked at. Therefore we cannot exclude an alternative explanation: the main low-degree pulsation mode that has been observed consistently from the 70's into the 90's, has damped out leaving no trace in our data taken in 1998.

5. Line-profile variations in ν Cen

5.1. Variations of the line-profile moments

To find the frequencies of the pulsations that presumably cause the line-profile variations we first analysed the variations of the profile moments (see e.g. Aerts et al. 1996, for the diagnostic value of moment variations for pulsation mode identification). From the orbit-corrected line profiles we calculated the first three velocity moments, as defined in S97. We computed the CLEANed Fourier transform (Roberts et al. 1987) of the velocity moments and the EW for both the λ 4552 and λ 4567 line.

We find that the resulting periodograms of the two lines are very noisy and are in general not consistent with eachother. EW variability peaks at low frequencies (between 0–0.6 d^{-1}) indicating that small EW variations may be linked to orbital phase. In all three velocity moments there is evidence for variability at frequencies ~2.35 and/or ~3.35 d^{-1}, which are one-day aliases.

5.2. Fourier analysis of the variability across the line profile

In order to find the pulsation frequencies we also analysed the time series with the method described by Gies & Kullavanijaya (1988) and S97. The method is based on the Doppler imaging principle (Vogt et al. 1987), in which one assumes a mapping of photospheric features (e.g. local velocity, brightness or EW variations) onto line profiles that are Doppler broadened by the rotation of the star. From a Fourier transform applied to each wavelength bin of a time series of observed spectra one obtains the power of variability as a function of frequency (periodogram), for all positions in the line profile. Additionally, the Fourier analysis provides information about the phase change of the periodic variations across the line profile. Using the power and phase information, a number of pulsation parameters can be derived.

The shortest timespan between subsequent exposures corresponds to a Nyquist frequency of ~50 d^{-1}. The length of the dataset is such that the *HWHM* of the main power peak in the window function is 0.047 d^{-1}. For each wavelength bin in the line profiles we Fourier-analysed the variable signal: we computed the Fourier components for frequencies between 0

and 50 d^{-1} with a frequency spacing of 0.01 d^{-1}. We CLEANed the resulting Fourier spectrum of each wavelength bin in order to remove the temporal window function, which is due to incomplete sampling of the variational signal. We used CLEAN parameters $N_{\rm iterations}$ = 400 and a gain of 0.2 (Roberts et al. 1987). For the SiIII λ 4552 line profile the resulting two-dimensional periodogram is displayed in Fig. 4.

The result of our Fourier analysis is again not in agreement with Rajamohan (1977), Kubiak & Seggwiss (1982), Ashoka (1985) and Ashoka & Padmini (1992), who find a single period of ~0.17 day in their radial velocity data. We do not find a dominant peak for periods between 0.156 and 0.195 day.

5.3. Towards the intrinsic frequency spectrum of ν Cen

Figure 5 shows the one-dimensional periodograms obtained by summing the variational amplitudes of the two-dimensional periodograms over the wavelength range which covers the line profiles. We find that the frequency spectra obtained from the SiIII λ4567 and λ4552 line profiles are very similar. The frequencies of the maxima detected in both lines differ less than 0.02 d^{-1}. We investigated the origin of the peaks in the periodograms.

5.3.1. One-day aliasing

Some of the power has obviously leaked to one-day aliases, which shows that the CLEAN algorithm was not able to fully correct for the window function. The peaks recognized as weak one-day aliases of other (stronger) frequencies are indicated by the thin vertical lines in Fig. 5. There are a few remaining ambiguities in the recognition of false peaks caused by aliasing, such as the pairs of peaks at frequencies 4.16 and 5.13 d^{-1}, and at 2.35 and 3.32 d^{-1}. For both these two pairs, one peak is most probably a one-day alias of the other.

Neglecting the weak one-day aliases, the remaining frequencies are 2.35, 3.32, 4.16, 4.66, 5.13, 6.42, and 7.95 d^{-1}. Peaks at frequencies below 2.0 d^{-1} are discarded (see Sect. 6.2). Based on the periodograms alone, we cannot decide whether all peaks at the above frequencies are real or that some are a result of data reduction, noise and/or insufficient data sampling.

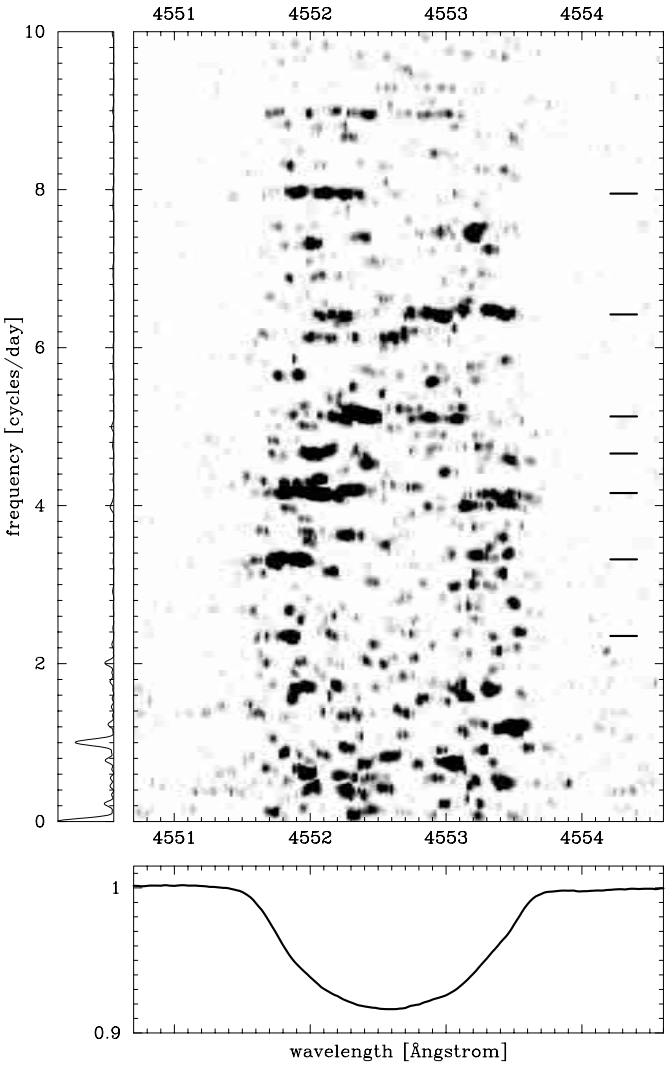

Fig. 4. Top: CLEANed Fourier analysis. For every wavelength bin (horizontal axis) a Fourier analysis of all the spectra is carried out. The power resulting from the Fourier analysis is plotted as a grey-value as a function of temporal frequency (vertical axis). Grey-scale cuts: 0–2 × 10^{-7}. Horizontal bars indicate the frequencies used in the further analysis. **Bottom:** Mean of all spectra. **Left:** Corresponding window function.

5.3.2. Iterative prewhitening

We iteratively prewhitened the time series using a single frequency for each iteration. We tried several series with different combinations of frequencies. We find that four iterations are sufficient to remove the seven most prominent peaks selected from the original summed periodogram. Different combinations of four frequencies lead to similar results. The frequencies 7.95 and 6.42 d^{-1} are required, plus either 4.16 or 5.13 d^{-1}, and 2.35 or 3.32 d^{-1}. We remove most power from the Fourier transform if we prewhiten with 5.13, 7.95, 2.35 and 6.42 d^{-1} (see Fig. 6).

We suspect that one pulsation mode is responsible for the two peaks at 2.35 and 3.32 d^{-1}, and another mode causes both peaks at 4.16 and 5.13 d^{-1}. Two other pulsation modes give rise to the peaks at 7.95 and 6.42 d^{-1}. The peak at 4.66 d^{-1} is automatically removed in the prewhitening process, and is most likely a by-product of the other frequencies. Most of the power at the weak one-day aliases (see Sect. 5.3.1) is removed in the four iterations, as expected.

We conclude that the intrinsic frequency spectrum of ν Cen consists of only 4 dominant frequencies, and that more data is needed to precisely determine the true intrinsic frequencies. For the rest of our analysis we have created diagnostic diagrams for each of the seven peaks selected from the summed periodogram. We keep in mind that only four peaks are real, and that the other three are artefacts.

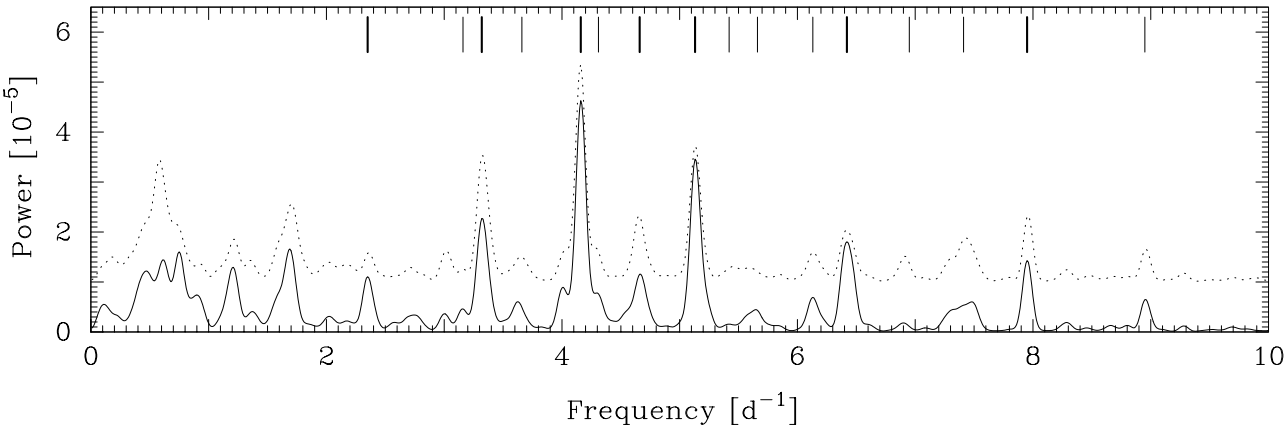

Fig. 5. Summed CLEANed Fourier spectrum. The power (i.e. the square of half the amplitude) in the two-dimensional periodograms of the λ4552 (solid) and λ4567 (dotted) lines has been summed over the line profile. The thick vertical lines indicate the frequencies used in the analysis while the peaks identified as weak one-day aliases are indicated by the thin vertical lines.

6. IPS amplitude and phase diagrams

In S97 we developed diagnostic tools for the analysis of non-radial pulsations in rotating stars, based on the IPS (Intensity Period Search) method (see also Gies & Kullavanijaya 1988). The method leads for each detected frequency to two diagnostic diagrams, the amplitude and the phase diagram, giving a full representation of the line-profile variations caused by each of the individual pulsation modes.

The two diagrams are very different and are each related to distinct properties of the pulsation mode. The amplitude diagram contains information on mode parameters like the ratio of horizontal to vertical pulsation amplitude k, inclination angle i, pulsational velocity amplitude $V_{\rm max}$, rotation parameter $\Omega/\omega^{(0)}$, intrinsic line width W, amplitude of temperature variations $(\delta T/T)_{\rm max}$, equivalent width response to temperature variations $\alpha_{W_{\rm E}}$ and non-adiabatic phase-lag $\chi^{\rm na}$ (see S97 and Schrijvers & Telting 1999, for further explanation of these symbols). The phase diagram is representative for the pulsation index ℓ (and $|m|$ if a harmonic is measured also). Telting & Schrijvers (1997, hereafter TS97) established a relation between the measured phase diagram and the ℓ value of the responsible pulsation mode.

Here, we use three different techniques to calculate IPS diagnostics for each of the suspected pulsation frequencies: single-sinusoid fits, multiple-sinusoid fits, and the CLEANed periodogram (Fig. 4). The top diagram in Figs. 8 and 9 displays the amplitude distribution across the line profile. The bottom diagram shows the phase distribution across the line profile. We present the amplitudes in units of $d_{\rm mean}$, which is the maximum absorption depth of the mean line profile, to allow a better comparison with theoretical models. For the λ4552 line we find $d_{\rm mean} = 0.084$ in continuum units. The wavelengths corresponding to $-V_{\rm e}\sin i$ and $V_{\rm e}\sin i$ are indicated by the marks on the bottom axis of the phase diagrams, were we used $V_{\rm e}\sin i = 65 \pm 6\,{\rm km\,s^{-1}}$ from Brown & Verschueren (1997).

For the region in which we find significant amplitude the amplitude and phase distributions are drawn with a solid line.

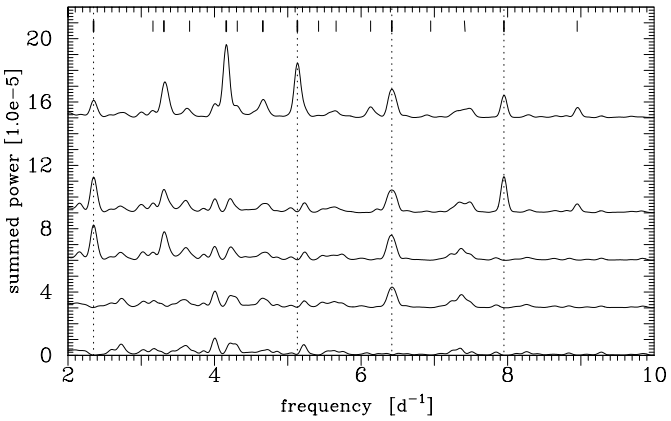

Fig. 6. Summed Fourier spectra after iteratively prewhitening with the frequencies of the strongest peaks. The isolated plot at the top shows the summed Fourier transform which is also shown in Fig. 5. The four lower plots show (from top to bottom) the summed Fourier transforms after subsequently prewhitening with 5.13, 7.95, 2.35 and 6.42 d^{-1}. These frequencies are indicated by the dotted vertical lines. The thick and thin vertical lines have the same meaning as in Fig. 5.

Outside this region a dotted line is used. The positions in the phase diagram at which we measure $\Delta\Psi$ are indicated by a square symbol.

6.1. IPS diagrams from the Fourier transform

We used the Fourier transforms from Sect. 5.2 (see Fig. 4) to investigate the amplitude and phase behavior across the line profile. For each of the 7 selected frequencies we plot the amplitudes and phases at each position in the line profile, leading to the IPS diagrams represented by the thinnest lines in Figs. 8 and 9.

Most of the IPS amplitude diagrams obtained from the Fourier transform appear non-continuous and some of the IPS phase diagrams show discrete jumps. Some of these diagrams are useless for mode-identification. We therefore adopted a second method to create the diagnostics.

6.2. IPS diagrams from the direct fit approach

We created IPS diagnostics by fitting sinusoids with fixed frequencies to the intensity variation at each position in the line profiles. The input frequencies were taken from the results of the Fourier analysis. The main advantage of this approach, when compared to creating IPS diagnostics from the CLEANed Fourier transform, is that it does not allow one-day aliases. At certain wavelengths the Fourier transform assigns all power to the one-day alias instead of the main peak, which leads to zero amplitudes and an irregular phase diagram at that position. This problem does not arise when creating IPS diagnostics by fitting sinusoids with fixed frequencies. We performed fits of the function

$$I(\lambda, t) = \sum_{i=1}^{N} A_i(\lambda) \sin(f_i t + \Psi_i(\lambda)) \quad (1)$$

to the intensity variations, where $A_i(\lambda)$ and $\Psi_i(\lambda)$ are the free parameters in the fit. The IPS diagnostics are created by plotting $A_i(\lambda)$ and $\Psi_i(\lambda)$ across the line profile.

For each of the 7 selected frequencies (Sect. 5.2) we created IPS diagrams in different ways. We applied a multiple-sinusoid fit (Eq. (1)) for the combination of 4 frequencies mentioned in Sect. 5.3.2, leading to an amplitude and phase diagram for each of these 4 frequencies (indicated by the lines with medium thickness in Figs. 8 and 9). Another set of diagnostics was created by fitting a single sinusoid to the variability, for each of the 7 individual frequencies (thick lines in Figs. 8 and 9).

For the frequencies below $2\,\mathrm{d}^{-1}$ we were not able to obtain IPS diagrams that are in some way similar to those generated with theoretical models of non-radial pulsations. We cannot decide whether these frequencies are caused by pulsations or other stellar phenomena or by observational effects. Part of these variations are probably due to variations arising from orbital and tidal phenomena, such as ellipsoidal variations and their spectroscopic equivalent. Other detected frequencies below $2\,\mathrm{d}^{-1}$ may be due to beating of the periodic signals at higher frequencies. From this point on we focus on the frequencies above $2\,\mathrm{d}^{-1}$.

6.3. Reconstruction of the time series

We used Eq. (1) to extract IPS amplitude and phase diagrams from the line profiles. We also used the IPS diagrams from the multiple-sinusoid fit to reconstruct the data by means of Eq. (1). The reconstruction, which is presented in Fig. 7, shows that 4 IPS diagrams give a reasonable representation of the most obvious variability. Note that including more frequencies in the multiple-sinusoid fit does not noticeably improve the reconstruction.

7. Mode identifications

We used three different methods to create the IPS diagnostics presented in Figs. 8 and 9. We find considerable differences between the diagnostics obtained with each of the three methods. Because of one-day aliasing, the amplitude diagrams created from the Fourier transform drop to zero at some positions within the line profile, which is reflected by the corresponding phase diagrams behaving irregularly at these positions. We attribute this to an insufficient sampling by our 93 spectra. The amplitude diagrams from the sinusoid fitting methods are not affected by one-day aliasing effects, which results in more realistic amplitude diagrams and more monotone phase diagrams. We find that the phase diagrams from the different methods are consistent in the ranges in the line profile where the corresponding amplitude diagrams are non-zero.

Note that the amplitudes from the Fourier transform are systematically lower than those from the fit methods. Apart from power that has leaked to one-day aliases, this is caused by the CLEAN algorithm which not only removes the window function from the periodogram but also some of the power at the real frequencies.

Amplitude diagrams are easily affected by problems like insufficient data sampling and imperfections of the data reduction. In contrast, the phase diagrams are rather robust. Regions in the line profile at which zero amplitude is found do not always hamper a correct retrieval of ℓ values for these modes. If the amplitude distribution is interrupted over only a short wavelength interval, it should be obvious whether the phase is connected correctly over the power-lacking region. A failure would result in a 2π jump that is clearly visible.

7.1. Determination of ℓ values

The IPS diagnostics derived for the 7 frequencies are displayed in Figs. 8 and 9. Non-radial pulsations give a plausible explanation for the variability displayed in these diagrams. In order to determine the degree ℓ of the pulsation modes, we measure for each frequency the maximum blue-to-red phase difference $\Delta\Psi$ from the phase diagrams, in the region of the line profile where we find significant amplitudes. We determined $\Delta\Psi$ for the IPS phase diagrams obtained by all three methods, i.e. Fourier transform, multiple-sinusoid fit and single-sinusoid fits. These values for $\Delta\Psi$ are listed in Table 1, provided that a useful phase diagram was obtained.

To estimate the pulsation degree ℓ from the maximum blue-to-red phase difference $\Delta\Psi$ we used one of the relations given by TS97. For the present analysis we chose to use the entry for modes with $\ell - |m| < 6$, for which they found an 84% certainty of retrieving the correct value of $\ell \pm 1$:

$$\ell = 0.015 + 1.109|\Delta\Psi|/\pi. \quad (2)$$

In some of the phase diagrams amplitude is missing at the line wings, i.e. the amplitude diagrams do not extend over a region larger than $2\times V_\mathrm{e} \sin i$. For these cases we obtain lower limits for $\Delta\Psi$, from which we derive a lower limit for ℓ. We also estimate the upper limit for ℓ by assuming that the phase diagram is symmetric around line center.

Table 1 lists the ℓ values derived with each of the 3 methods and for all selected frequencies, as well as our final ℓ determinations.

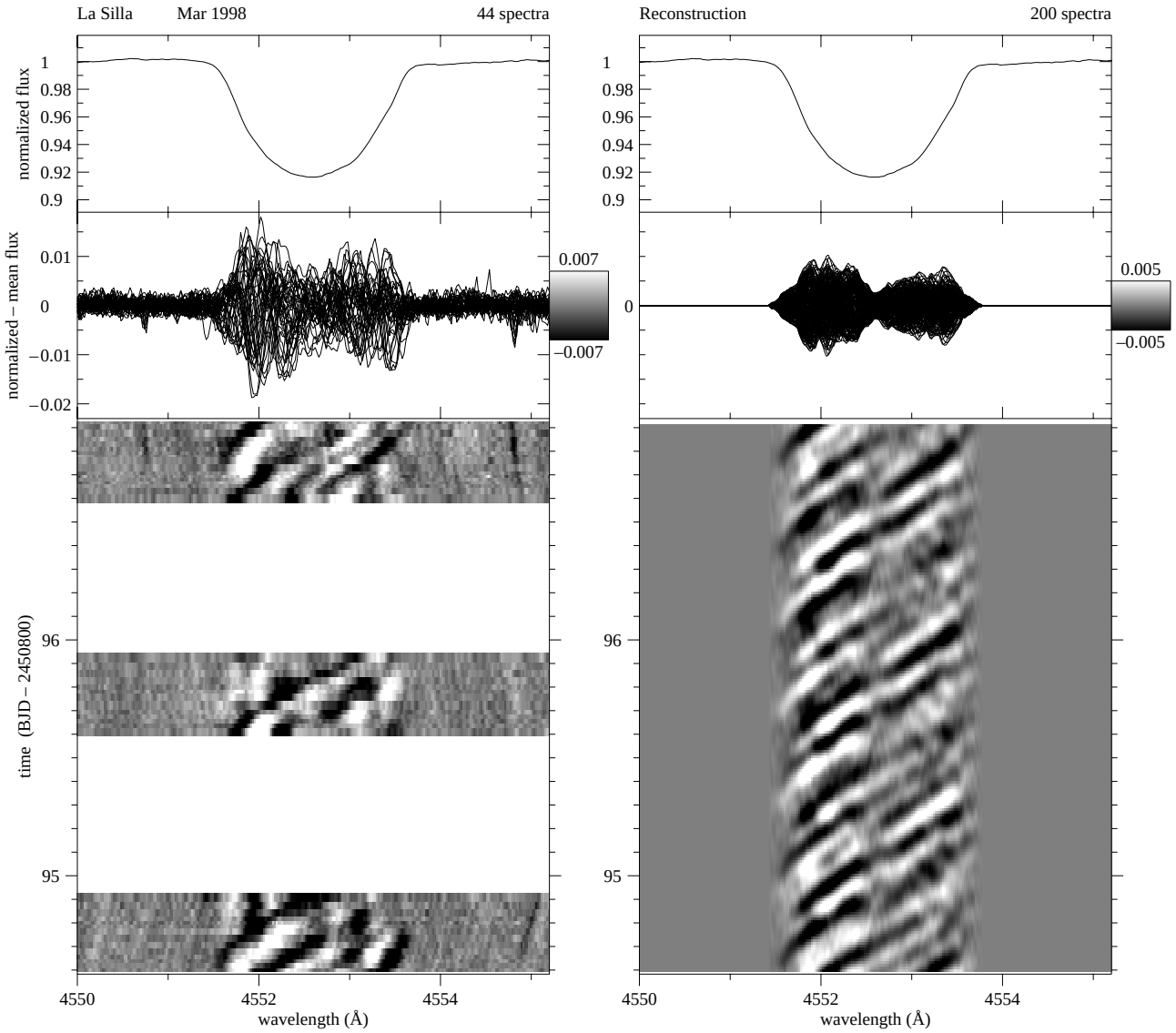

Fig. 7. Left: Last three nights of the observed time series of the λ 4552 Å line profile. Bottom: gray-scale representation of residual spectra (mean subtracted). Intensities less than average are indicated black; bright regions in the profile are indicated by lighter shades. Middle: Overplot of all residuals. This panel shows that most of the variability is present at the wings of the line profile. Top: Mean of all line profiles. **Right:** Reconstruction of data from the IPS diagrams resulting from our multiple-sinusoid approach. We used the IPS diagrams at 2.35, 5.13, 6.42 and 7.95 d^{-1} to reconstruct the data covering the last three nights. This figure illustrates that the data is well represented by 4 IPS diagrams. Including more than 4 frequencies in the multi-sinusoid fit does not lead to a noticable improvement of the reconstruction.

1) Line-profile variations with $f = 4.16$ and $f = 5.13\,d^{-1}$

At both these frequencies, which are one-day aliases, we find amplitude and phase diagrams which extend over the full wavelength domain between $-V_e \sin i$ and $+V_e \sin i$.

Although we expect that only one pulsation mode is responsible for the detection of these two frequencies, we nevertheless derive ℓ values for both these frequencies. From $\Delta\Psi^{SF}$ we estimate $\ell = 6$ for the mode that is responsible for $f = 4.16$ and $f = 5.13$.

2) Line-profile variations with $f = 4.66\ d^{-1}$

The diagnostics calculated at $4.66\,d^{-1}$ show a non-monotonic phase diagram which is inconsistent with those predicted theoretically: we do not find much amplitude in the red half of the line profile. This frequency might be the result of beating between 3.32 and 7.95 d^{-1}. The variability with frequency $4.66\,d^{-1}$ is removed when prewhitening with the other frequencies, and we regard it unlikely that $4.66\,d^{-1}$ is one of the intrinsic frequencies in ν Cen.

3) Line-profile variations with $f = 7.95\,d^{-1}$

For the diagnostics from the CLEANed Fourier transform, amplitude seems missing at the red wing of the line profile, and the phase diagram behaves erratically in the red half of the line profile. The diagnostics from the single-sinusoid and multiple-sinusoid fits do not have this problem. We find $\ell = 10$ for this frequency.

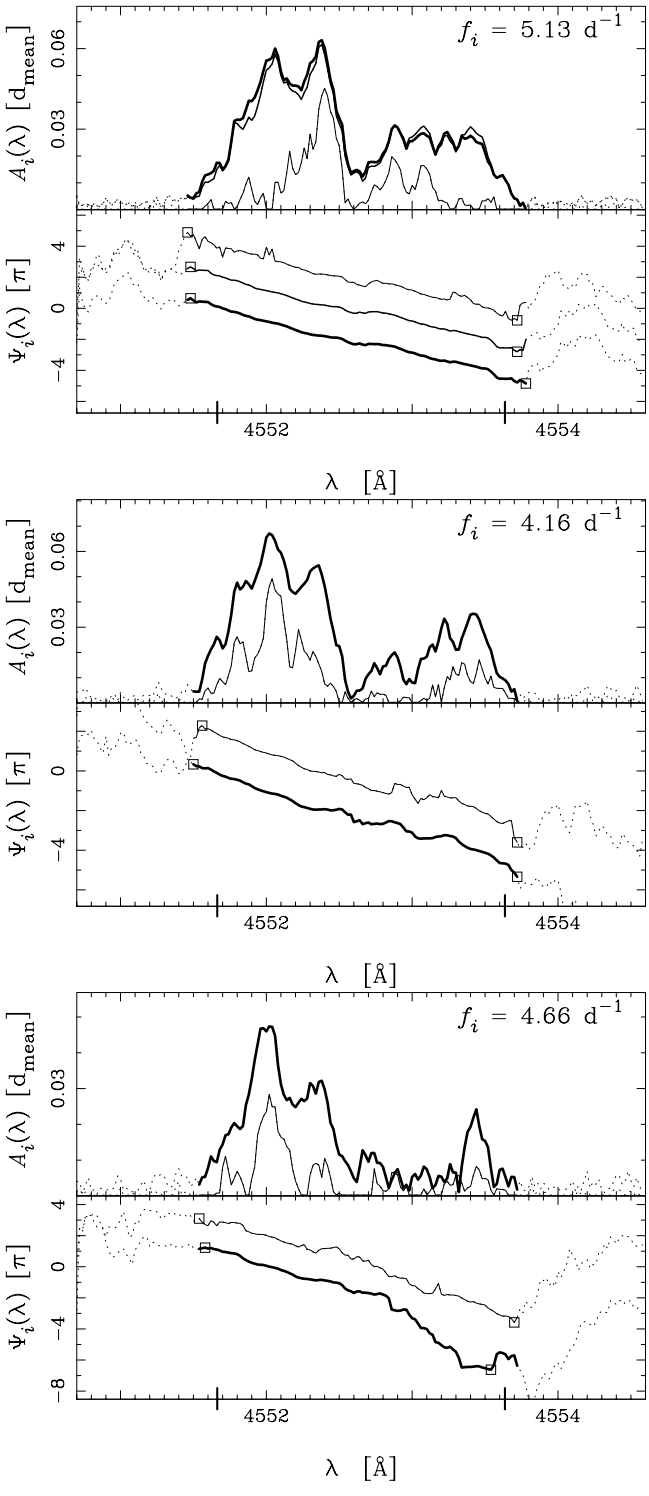

Fig. 8. IPS diagnostics for the variations found in the λ4552 line profile at the frequencies 5.13, 4.16 and 4.66 d^{-1}. See Sect. 6 for a general description of the diagrams. Heavy line: single-sinusoid fit, thinner line: multiple-sinusoid fit, thinnest line: CLEANed Fourier transform.

4) Line-profile variations with $f = 6.42\,\mathrm{d}^{-1}$

At this frequency it appears as if amplitude is missing close to the line center and at the blue wing of the line profile. Around the line center there seems to be no problem with the phase diagram, but around – $V_\mathrm{e} \sin i$ part of the phase diagram is missing (see Sect. 7). The phase diagrams at 6.42 d^{-1} give rise to a lower limit for ℓ.

We estimate that our measured value for $\Delta\Psi^{\mathrm{SF}}$ underestimates the true blue-to-red phase difference by not more than π. This yields a pulsation mode with $\ell = 7$ or $\ell = 8$ for this frequency.

5) Line-profile variations with $f = 2.35$ and $f = 3.32\,\mathrm{d}^{-1}$

The IPS diagrams obtained for 2.35 and 3.32 d^{-1} are far from ideal. Amplitude is missing in the red half of the line profile and in the corresponding region the phase diagrams show irregular behavior, instead of a smooth and gradual change as expected for non-radial pulsations. Therefore the ℓ value that we derive for this presumed mode is tentative.

We derive $\ell < 6$ from the phase diagrams at 2.35 and 3.32 d^{-1}. The facts that these frequencies show up in the analysis of the first three velocity moments (see Sect. 5.1) and that the phase diagrams are irregular, hint at a lower ℓ value for this pulsation mode that is most probably tesseral.

Note that 3.32 d^{-1} is, within the half width of the main peak of the window function (0.047 d^{-1}), the beat frequency of 4.66 and 7.95 d^{-1}. This might indicate that 3.32 and 7.95 d^{-1} are true frequencies and that 2.35 d^{-1}is a one-day alias of 3.32 d^{-1}.

8. Multiple pulsation modes in ν Cen

In the previous section we analysed the amplitude and phase characteristics of the line-profile variability in ν Cen. We assumed that the variability is caused by multiple non-radial pulsation modes, and derived an ℓ value for each of the presumed pulsation modes. In this section we address whether the assumption of non-radial pulsations is supported by the observations. We discuss some of the implications.

To investigate the parameter space of the pulsation modes we consider three scenarios regarding the rotation rate of ν Cen, relative to the orbital frequency. For the first scenario, ν Cen has been tidally synchronized by the companion, i.e. the rotation period is equal to the orbital period. Based on published values for some of the stellar parameters ($R = 6.7\,R_\odot$, $V_\mathrm{e} \sin i = 65$ km s^{-1}) we find an inclination $i = 30.22°$, rotational velocity $V_\mathrm{e} = 129$ km s^{-1}, and a rotation rate $\Omega = 0.38\,\mathrm{d}^{-1}$ for the case of synchronous rotation. For the second scenario we take a sub-synchronous rotation by assuming $i = 60°$, which gives $V_\mathrm{e} = 75$ km s^{-1} and $\Omega = 0.22\,\mathrm{d}^{-1}$. Super-synchronous rotation is accounted for by the third scenario of $i = 20°$, which implies $V_\mathrm{e} = 190$ km s^{-1} and $\Omega = 0.56\,\mathrm{d}^{-1}$. For these three considered cases we use $\omega = f_\mathrm{obs} - |m|\Omega$ to calculate lower limits for the intrinsic pulsation frequencies. The lower limit ω_lo is the frequency for prograde sectoral modes ($m = -\ell$); tesseral modes imply frequencies higher than ω_lo. We use the lower limit of the frequency to calculate an upper limit for the ratio of the horizontal to vertical pulsational surface motions, $k = \frac{GM}{R^3\omega^2}$, using $M = 13\,M_\odot$ from Remie & Lamers (1982). The values for the lower limits ω_lo and upper limits k_up, calculated for the three scenarios, are listed in Table 2.

It is interesting to note that from the mass function, assuming $M_1 = 13\,M_\odot$, it follows that the lower limit of the

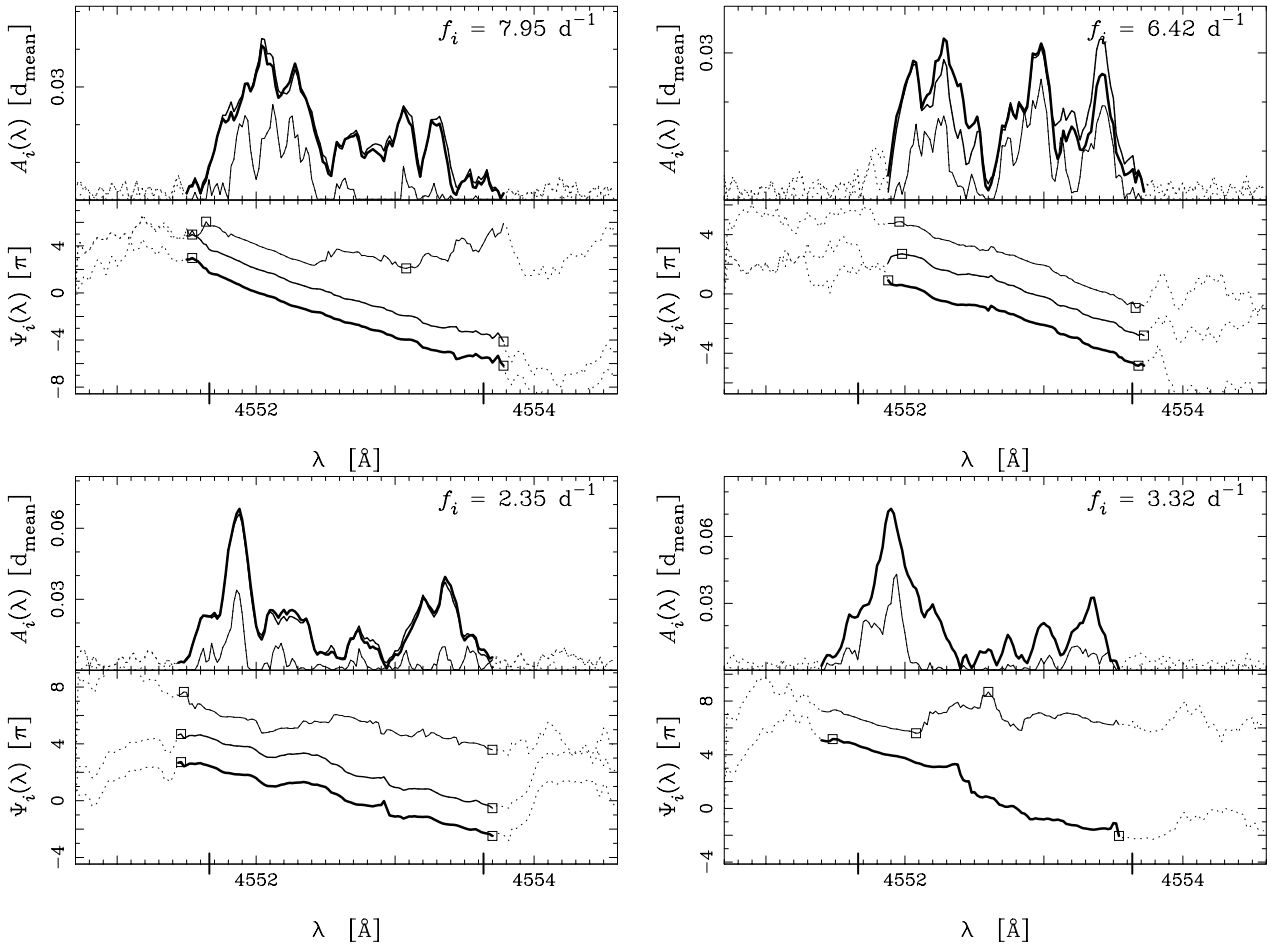

Fig. 9. Similar to Fig. 8, but for the frequencies 7.95, 6.42, 2.35 and 3.32 d^{-1}. See Sect. 6 for a general description of the diagrams.

companion mass is $M_2 \geq 0.8\ M_\odot$. For assumed orbital inclinations of $i_{\rm orb} = 60, 30.22, 20°$ it follows that $M_2 = 1.0, 1.7, 2.7\ M_\odot$ respectively.

One should keep in mind that the brightness varies with the orbital period (ellipsoidal variations, Waelkens & Rufener 1983; Cuypers et al. 1989), implying that the orbital inclination cannot be too low.

8.1. Frequency considerations

It is generally accepted that non-radial pulsations are a common feature of β Cephei stars. The excitation mechanism for pulsations in these stars is firmly established to be the κ-mechanism (Moskalik & Dziembowski 1992; Gautschy & Saio 1993; Dziembowski & Pamyatnykh 1993).

We investigate if the observed frequencies agree with the theoretically predicted frequencies in the corotating frame. Figures 5 and 6 of Dziembowski & Pamyatnykh (1993) show that pulsation modes with $\ell < 6$ can only be p modes, whereas modes with $\ell \geq 6$ can be both p-type and g-type oscillation (for their β Cephei model with $M = 12\ M_\odot$). The predicted frequency domains for their β Cephei star model are $\omega \leq 2.6\,{\rm d}^{-1}$ for the g modes and $\omega \geq 5.6\,{\rm d}^{-1}$ for the p modes (assuming $R = 6.7\ R_\odot$). For all our modes we derived $\ell \gtrsim 6$ which suggests that both p- and g-mode instability can be expected in ν Cen. For modes for which we have two possible frequencies, we consider both possibilities.

Of course, since the frequencies listed in Table 2 are lower limits, all modes could be p modes if we allow only tesseral modes. Another possibility is that all frequencies in ν Cen are g modes. Of our three scenarios in Table 2, only the super-synchronous rotation ($i = 20°$) leads to frequencies that are all in the theoretically expected range for g modes.

Note the commensurability of the frequencies 5.13 and 6.42 d^{-1} which have a ratio of 4:5. This can be a coincidence but if the $|m|$ values of the two responsible pulsation modes have the same ratio this would mean that the two modes have identical superperiods. It could be advocated that these two frequencies are multiples of the rotation frequency. We checked for an equivalent period ratio that would match more than two commensurate frequencies. We find that the ratios 26:29:32:40 matches 4 of the frequencies very well (4.168:4.649:5.130:6.413 d^{-1}). However, we regard it as unlikely that such a ratio would be a real rotationally induced phenomenon: the implied rotation rate would be $\Omega = 0.16\,{\rm d}^{-1}$, leading to $R > 8\ R_\odot$.

We investigate whether the observed set of 7 frequencies is consistent with tidally induced pulsations. In this case the frequencies in the observers frame should be multiples of the orbital frequency $f_{\rm orb} = 0.381\,{\rm d}^{-1}$ (see also Telting et al. 2001).

Table 1. The frequencies found in the summed Fourier transform of the SiIII λ4552 line profile ordered according to their power (see Fig. 5). The first column lists the frequency in d^{-1}. The second gives the period in hours. The maximum blue-to-red phase differences $\Delta\Psi$ measured from the IPS diagnostics calculated from the Fourier transform (label FT), the multiple-sinusoid fit (label MF) and the single-sinusoid fits (label SF), are listed in Cols. 3–5 (in units of π radians). Columns 6–8 list the fractional ℓ values calculated from Cols. 3–5 by means of Eq. (2). The two rightmost columns list the values for $\Delta\Psi$ (in π radians) and ℓ from our final interpretation of the diagnostics; these were the results of careful consideration of all amplitude and phase diagrams.

$f_{\rm obs}$	$P_{\rm obs}$	$\Delta\Psi^{\rm FT}$	$\Delta\Psi^{\rm MF}$	$\Delta\Psi^{\rm SF}$	$\ell^{\rm FT}$	$\ell^{\rm MF}$	$\ell^{\rm SF}$	$\Delta\Psi$	ℓ
2.35	10.21	4.07	5.21	5.20	–	5.8	5.8	<5.2	<6
3.32	7.23	3.08	–	7.22	–	–	–	–	–
4.16	5.77	5.89	–	5.67	6.6	–	6.3	5.7	6
4.66	5.15	6.68	–	7.85	–	–	–	–	–
5.13	4.68	5.67	5.46	5.49	6.3	6.1	6.1	5.5	6
6.42	3.74	5.84	5.52	5.80	6.5	6.1	6.4	>6.0	>7
7.95	3.02	3.97	9.09	9.15	–	10.1	10.2	9.1	10

The length of our dataset is such that the error on our frequency determinations is a considerable fraction of the orbital frequency: from the *HWHM* of the main peak of the window function we find that $\sigma = HWHM/1.177 = 0.04\,d^{-1}$ (assuming the peak is Gaussian). Only observed frequency $5.13\,d^{-1}$ is more than 3σ away from a multiple of the orbital frequency; only frequency $4.16\,d^{-1}$ (probably a one-day alias of $5.13\,d^{-1}$) is within 1σ from a multiple of the orbital frequency. We conclude that given the temporal resolution of our observations we cannot make conclusive statements about the possible tidal nature of these frequencies. Nevertheless we find that none of the observed frequencies is an exact match with a multiple of the orbital frequency. In Sect. 6.2 we have indicated that there may be evidence for orbital or tidal phenomena in the profile variations at low frequencies. Data taken over a significantly longer time base is needed to confirm this.

8.2. The k values of the modes

In contrast to the observed frequencies, it is less easy to bring the derived diagnostic diagrams in line with the pulsation interpretation. Contrary to what is theoretically expected, the amplitude diagrams appear discontinuous. However, with 93 spectra, this could well be caused by a sampling that is insufficient for the multiperiodic variations. We folded the acquisition times with the inverse of each of the 7 frequencies to investigate the sampling of each of the signals. We find that the phases corresponding to the acquisition times are well dispersed. However, the beat frequencies of neighboring frequencies are not properly sampled by the data set. This may explain the decreased or missing amplitude in some areas of the amplitude diagrams.

The observed amplitudes are obviously larger near the line wings than around the line center. This is clearly visible in the overplot of residual (mean subtracted) profiles in Fig. 7. Standard models of non-radial pulsations can only explain such behavior if the modeled ratio of the horizontal to the vertical motions, k, is substantial (say $k > 0.3$ implying g-mode pulsations), or if there are significant pulsational temperature variations with a negative response of the equivalent width (a negative value of $\alpha_{W_{\rm E}}$, see Telting & Schrijvers 1999, their Fig. 3).

Table 2. For the 3 scenarios of synchronous, sub-synchronous and super-synchronous rotation we calculated the lower limit for the pulsation frequency $\omega_{\rm lo}$ and the upper limit $k_{\rm u}$. The case marked with $\star$ indicates the exception of a retrograde mode for $|m| = \ell$. The values depend on the observed frequencies and ℓ values (see Table 1) and on estimates for the mass and radius of ν Cen ($M = 13\ M_\odot$, $R = 6.7\ R_\odot$, $V_{\rm e} \sin i = 65\ {\rm km\,s^{-1}}$).

		super-synchr. $i = 20°$		synchronous $i = 30.22°$		sub-synchr. $i = 60°$	
f_i	$\lvert m\rvert$	$k_{\rm u}$	$\omega_{\rm lo}$	$k_{\rm u}$	$\omega_{\rm lo}$	$k_{\rm u}$	$\omega_{\rm lo}$
2.35	≤6	3.3	0.99*	842	0.062	3.07	1.02
4.16	≤6	4.8	0.82	0.92	1.87	0.40	2.83
5.13	≤6	1.0	1.79	0.40	2.84	0.22	3.80
6.42	≤8	0.83	1.96	0.28	3.37	0.15	4.65
7.95	≤10	0.57	2.38	0.19	4.14	0.10	5.74

Although the amplitude diagrams deviate strongly from the ideal cases, we have the impression that some of the amplitude diagrams agree more with high k values than others. The amplitude diagrams for the presumed pulsation modes at 7.95, 6.42 and $5.13\,d^{-1}$ appear to have more amplitude around the line center than those at 2.35, 3.32, 4.16 and $4.66\,d^{-1}$. As evidenced by Table 2 this would agree perfectly with the concept of pulsations: the higher k values expected for the modes with the lower frequencies seem to be sustained by the amplitude diagrams.

The quality of our amplitude diagrams is not high enough to really estimate the k values of the modes, which would lead to an estimate of the stars rotation rate Ω. However, the low k values expected for the case of sub-synchronous rotation seem less compatible than the other two cases (see Table 2).

8.3. Harmonic variability due to high pulsational velocity amplitudes

We did not find harmonic variability (i.e. $2f_{\rm obs}$) for any of the investigated frequencies. Harmonics are expected to show up for large line-profile variations if the contribution of velocity fields to the variations, as opposed to the effects of local brightness and EW variations, is large enough

(Schrijvers & Telting 1999). The fact that we do not find harmonics does however not make non-radial pulsations a less probable explanation for the observed variability. In fact, for the observed line-profile amplitudes (less than 6% of the absorption depth of the mean line profile $d_{\rm mean}$) it would be very hard to detect such harmonics, even if the line-profile variations are solely caused by surface velocity fields.

A consequence of the harmonics remaining undetected is that we only have an upper limit $|m| \leq \ell$, rather than retrieving $|m|$ from the phase diagram of the harmonic.

8.4. Spectroscopic versus photometric variations

Small-amplitude light variations, with period 0.17 day, were presented by Kubiak & Seggwiss (1982, $\Delta u = 8$ mmag). These authors did not find variations in the other Strömgren bands. Cuypers et al. (1989) found photometric (Strömgren b) variations in ν Cen showing the orbital period known from spectroscopy. They looked for the possibility of other frequencies, but their careful investigations did not reveal any sign of variations at other frequencies, with amplitudes exceeding 2 millimags.

The result of the present work makes clear the potential of spectroscopic pulsation searches: it turns out that in 1998 ν Cen exhibited pulsation modes with only intermediate ℓ values, and light variations related to such high ℓ values are simply too small to be detected.

This emphasizes that we are in an era of finding new β Cephei variables spectroscopically, rather than photometrically. Of all nearby β Cephei stars, most of the photometric variables are already known, whereas many line-profile variables might still be undiscovered.

9. Tidal interactions in close-binary β Cephei stars

Waelkens & Rufener (1983) searched for pulsations in photometric observations of close binaries containing early-B type stars, and concluded that for close binaries with periods shorter than that of α Vir (orbital period $P = 4.0$ day, eccentricity $e = 0.15$, pulsations in the primary, Smith 1985) no pulsations are detectable, and argued that in close binaries the tidal forces may suppress the β Cephei pulsations. With their photometric observations they could only detect low degree modes. However, they did not detect a low degree mode in ν Cen at the time.

The present work on ν Cen shows, however, that β Cephei stars with shorter orbital periods do exist. Another case was presented by Telting et al. (2001) for the star ψ^2 Ori, which has an orbital period $P = 2.53$ day. The moving bump pattern in the primary of this binary with low eccentricity ($e = 0.05$) can be explained by two non-radial pulsation modes with $\ell \sim 6$. This means that in ψ^2 Ori, ν Cen, and α Vir, which are the three β Cephei stars with closest known orbits, non-radial pulsations have been detected spectroscopically.

It is clear that the conclusion put forward by Waelkens & Rufener (1983) does not hold, but it is still unclear if the tidal forces in close binaries can cause the amplitudes of low-degree β Cephei pulsations to damp out or become variable. For ν Cen and α Vir there is strong observational evidence that a low-degree (non-)radial mode has damped out. A possible variable-amplitude low-degree mode in ν Cen (Ashoka & Padmini 1992) giving rise to radial velocity variations of about 10 km s^{-1} (20 km s^{-1} peak-to-peak) from 1985 to 1988, could not be detected in our high-S/N data set, obtained in 1998. Smith (1985) discussed the pulsational history of α Vir, in which the radial mode showed amplitude and phase variations and damped out.

Given these observations we argue that tidal interactions might have an impact on the amplitudes of the low-degree modes in β Cephei stars. It is also worth noting that both stars have fairly high equatorial rotation velocities (ν Cen primary: $100 \lesssim V_{\rm e} \lesssim 200$ km s^{-1}; α Vir primary: $V_{\rm e} \sim 175$ km s^{-1}). Suppression of radial modes was found to be the case for (single) rapid rotators (Ushomirsky & Bildsten 1998).

10. Conclusions

The main conclusions of this paper can be summarized as follows.

We observed complex line-profile variability in ν Cen. We Fourier analysed the line-profile variations and found variational power at a number of different frequencies. Many of these could be identified as one-day aliases of other frequencies.

We find no trace of a possible pulsation mode with $P = 0.17$ day in ν Cen. This previously reported low-degree mode must either have damped out, or it never existed. In the latter case the previous low-resolution spectroscopic observations must have been misinterpreted due to poor temporal sampling and low dispersion.

We find four non-radial pulsation modes in ν Cen and derive ℓ values between $\ell = 6$ and $\ell = 10$ for three of them.

The frequency spectrum of ν Cen remains partly unresolved. We found that only 4 frequencies are sufficient to reproduce the observed variability, but we were unable to firmly identify the true frequencies. For this, more extensive observations of ν Cen are needed, preferably from continuous multi-site observations since this prevents the appearance of one-day aliases in the frequency spectrum.

We conclude that non-radial pulsations do exist in β Cephei stars in very close orbits, and that the disappearance of low-degree modes in such stars may be related to tidal effects.

Acknowledgements. We thank Huib Henrichs and Jan van Paradijs for many helpful suggestions after carefully reading the first versions of the manuscript. We feel unable to express our gratitude to Jan, for his support throughout our undergraduate years, and for his courage and love during the last months of his life.

References

Aerts, C. 1996, A&A, 314, 115
Ashoka, B. N., & Padmini, V. N. 1992, Ap&SS, 192, 79
Ashoka, B. N., Surendiranath, R., & Kameswara Rao, N. 1985, Acta Astr., 35, 395
Brown, A. G. A., & Verschueren, W. 1997, A&A, 319, 811

Cuypers, J., Balona, L. A., & Marang, F. 1989, A&AS, 81, 151
De Cat, P., Telting, J. H., Aerts, C., & Mathias, P. 2000, A&A, 359, 539
De Geus, E. J., De Zeeuw, P. T., & Lub, J. 1989, A&A, 216, 44
De Zeeuw, P. T., Hoogerwerf, R., de Bruijne, J. H. J., et al. 1999, AJ, 117, 354
Dziembowski, W. A., & Pamyatnykh, A. A. 1993, MNRAS, 262, 204
Gautschy, A., & Saio, H. 1993, MNRAS, 262, 213
Gies, D. R., & Kullavanijaya, A. 1988, ApJ, 326, 813
Hendry, E. M., & Bahng, J. D. R. 1981, J. Astrophys. Astron., 2, 141
Kubiak, M., & Seggwiss, W. 1982, Acta Astr., 32, 371
Lucy, L. B., & Sweeney, M. A. 1971, AJ, 76, 544
Moskalik, P., & Dziembowski, W. A. 1992, A&A, 256, L5
Palmer, H. K. 1906, Lick Obs. Bull., 4, 97
Rajamohan, R. 1977, Kodaikanal Obs. Bull. Ser., A. 2, 6
Remie, H., & Lamers, H. J. G. L. M. 1982, A&A, 105, 85
Roberts, D. H., Lehár, J., & Dreher, J. W. 1987, AJ, 93, 968
Schrijvers, C., Telting, J. H., Aerts, C., Ruymaekers, E., & Henrichs, H. F. 1997, A&AS, 121, 343
Schrijvers, C., & Telting, J. H. 1999, A&A, 342, 453
Smith, M. A. 1985, ApJ, 297, 206
Sterne, T. 1941, Proc. Nat. Acad. Sci. Am., 27, 175
Telting, J. H., & Schrijvers, C. 1997, A&A, 317, 723
Telting, J. H., Abbott, J. B., & Schrijvers, C. 2001, A&A, 377, 104
Ushomirsky, G., & Bildsten, L. 1998, ApJ, 497, L101
Vogt, S. S., & Penrod, G. D., & Hatzes, A. P. 1987, ApJ, 496, 127
Waelkens, C., & Rufener, F. 1983, A&A, 121, 45
Wilson, R. E. 1914, Lick Obs. Bull., 8, 130
De Zeeuw, P. T, Hoogerwerf, R., de Bruijne, J. H. J., Brown, A. G. A. & Blaauw, A. 1999, AJ, 117, 354